Received December 26, 2017, accepted January 29, 2018, date of publication February 12, 2018, date of current version March 19, 2018.

Digital Object Identifier 10.1109/ACCESS.2018.2805463

Independently Tunable Concurrent Dual-Band VCO Using Square Open-Loop Resonator

BOQIONG LI[1], YONGLE WU[2], (Senior Member, IEEE), CUIPING YU[1], AND YUANAN LIU[1]

[1]Department of Electronic Engineering, Beijing Key Laboratory of Work Safety Intelligent Monitoring, Beijing University of Posts and Telecommunications, Beijing 100876, China

[2]State Key Laboratory of Information Photonics and Optical Communications, School of Electronic Engineering, Beijing University of Posts and Telecommunications, Beijing 100876, China

Corresponding author: Yongle Wu (wuyongle138@gmail.com).

This work was supported in part by the National Natural Science Foundations of China under Grant 61671084, Grant 61422103, and Grant 61327806, in part by the Fund of State Key Laboratory of Information Photonics and Optical Communications (Beijing University of Posts and Telecommunications), China, in part by the National Key Basic Research Program of China (973 Program) under Grant 2014CB339900, and in part by the Young Elite Scientists Sponsorship Program by CAST under Grant YESS20150118.

ABSTRACT A concurrent dual-band voltage-controlled oscillator (VCO) with independently tunable dual oscillation frequencies is proposed. A shared square open-loop dual-mode resonator and two varactor diodes are the basic units offering flexible tuning for the dual-band operation. A back-to-back varactor diode between the split of the resonator controls the odd-mode resonant frequency, and a single varactor diode is placed at the center of the resonator to adjust the even-mode resonant frequency. By combining the other four resonators with the shared dual-mode resonator, two distinct three-pole tunable bandpass filters (BPF) are designed as two frequency selective elements. Based on the two elements, a parallel-feedback concurrent dual-band VCO is fabricated with independently-tuned dual oscillation frequencies. Moreover, the mathematical deductions are analyzed to optimize the tuning ranges of the dual-oscillation frequencies and the circuit sizes. The measured results show that the two oscillation frequencies cover a tuning range of 5.114–5.28 GHz and 7.61–7.97 GHz, respectively.

INDEX TERMS Dual-band filter, open-loop resonator, concurrent dual-band VCO, independently tunable dual-band VCO.

I. INTRODUCTION

The concurrent multi-band and multi-mode transceiver with independently controllable capability is a trend in modern wireless communication systems. Accordingly, radio frequency (RF) and microwave components are required to achieve multi bands with flexible tuning characteristics. Oscillators, the vital RF and microwave device to provide carrier frequencies for the RF transceivers, have been investigated in response to this need. For instance, switchable dual-band resonator is commonly used in the design of dual-band oscillators [1]–[3]. The operation frequencies of these dual-band oscillators can be produced by switching devices, but they cannot operate simultaneously.

In order to replace the switching devices and support concurrent dual-band outputs, several concurrent dual-band BPFs acted as two frequency stabilization elements have been proposed to realize concurrent dual-band oscillators [4]–[9]. Due to the advantages of simplicity, concurrence and size reduction in the published dual-band BPFs including substrate integrated waveguide (SIW) resonators [4], $\lambda/4$ resonators [5], ring resonators [6], SIW split ring resonators [7], and LC resonators [8], these design approaches are the available alternatives for designing the concurrent dual-band VCOs. However, unwanted harmonic-mixing signals appear in the spectrum output around the needed oscillation frequencies [4], [5]. This is because the spurious suppressions of these dual-band BPFs are insufficient to suppress nonlinear mixing components. The problem is solved by utilizing the filtering dual-band BPFs reported in [6] and [7], which have sufficient spurious suppressions and high band-to-band isolations. As a result, taking the excellent performances of band-to-band isolation and spurious suppression into account is essential to develop concurrent dual-band VCOs.

Another notable issue to study is the independent control of the two oscillation frequencies. Some concurrent dual-band VCOs are adjusted over the wide ranges [8], [9], but two oscillation frequencies are highly affected by each other, since the two bands of the presented dual-band BPFs are determined by the same tuning device and are not independently generated. In [10], a concurrent dual-band VCO with flexible tuning characteristic has been realized based on a common four-pole dual-band resonator. However, the coupling theory of the dual-band VCO is a holistic form and leads to an inflexible implementation on ameliorating frequency selectivity of two bands. In this context, a new coupling scheme is introduced to freely improve the frequency selectivity for higher quality factors (Q).

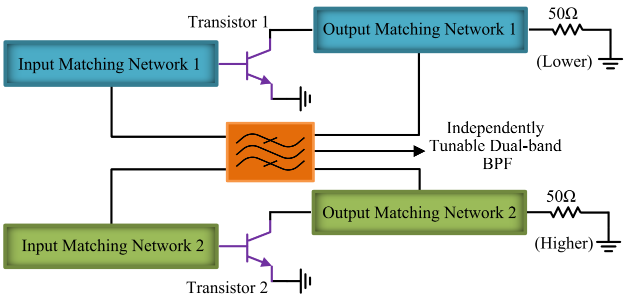

FIGURE 1. Block diagram of the proposed concurrent dual-band VCO.

In this paper, a novel concurrent dual-band VCO with independent control of the two oscillation frequencies is presented. The block diagram of the proposed concurrent dual-band VCO is shown in Fig. 1. The odd- and even-mode resonant frequencies of the developed dual-band BPF are treated as two bands and can be individually tuned by different varactor diodes. The dual-band BPF is connected with two transistors working at the different oscillation conditions to construct a concurrent dual-band VCO. Owing to the good band-to-band isolation and adequate spurious suppression, the dual-band BPF decreases the nonlinear mixing spurs so that the concurrent dual-band VCO achieves a pure spectrum output. Additionally, according to the principle of independent dual-band characteristic, theoretical analyses are explained to provide an effective criterion for circuit reduction and tuning range extension in the design of concurrent dual-band VCO.

II. THEORY FOR INDEPENDENT DUAL-BAND CHARACTERISTICS

A. INDEPENDENT TUNING ANALYSIS FOR ODD MODE AND EVEN MODE

Fig. 2(a) shows a one-pole square open-loop stepped-impedance (SI) resonator with characteristic admittance of Y_1 and Y_2, corresponding to physical length of L_1 and L_2 (assuming $L_1 = L_2 = L$), respectively. The resonator can be used for the shared dual-mode resonator by embedding a variable capacitance C_o between the split of the loop with two identical capacitances C, and placing a variable capacitor C_e at the center of the line. Due to the symmetrical structure of the shared dual-mode resonator, the use of the odd- and even-mode analysis method as described in [11] is suitable for deriving the dual-mode resonant frequencies.

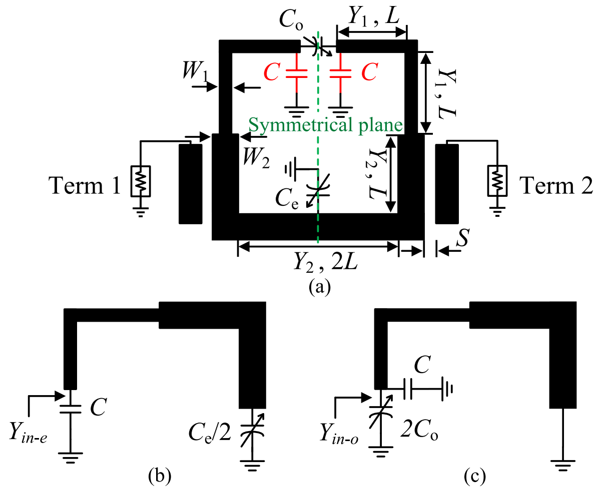

FIGURE 2. (a) A square dual-mode resonator. (b) Equivalent even-mode circuit. (c) Equivalent odd-mode circuit.

For the even-mode case, the symmetrical plane represents an open-circuited condition, as seen in Fig. 2(b). The even-mode resonant frequency f_e is calculated as

$$f_e^2 + \frac{f_e}{2\pi} \cdot \frac{\left(C_e Y_1^2 + 2CY_2^2\right)\tan^2(2L\beta_e) - Y_1 Y_2 (2C + C_e)}{C \cdot C_e (Y_1 + Y_2)\tan(2L\beta_e)} - \frac{Y_1 Y_2}{2\pi^2 C \cdot C_e} = 0, \quad (1)$$

where β_e is the even-mode propagation constant.

Likewise, for the odd-mode case, the symmetrical plane stands for a short-circuited condition, as seen in Fig. 2(c). The odd-mode resonant frequency f_o can be given as

$$f_o = \frac{Y_1 Y_2 - Y_1^2 \tan^2(2L\beta_o)}{2\pi (2C_o + C)(Y_1 + Y_2)\tan(2L\beta_o)}, \quad (2)$$

where β_o is the odd-mode propagation constant.

Observing from (1) and (2), f_e depends on C_e and C, and f_o is decided on C_o and C. It is noteworthy that if C is a given value, f_o and f_e are only determined by C_o and C_e, respectively. Consequently, f_o can be separately controlled without affecting f_e by varying C_o, and f_e can be independently tuned without disturbing f_o by varying C_e.

B. DUAL-BAND TUNING RANGE ANALYSIS

In addition to the independent regulation of dual-resonant frequencies, the research on tuning range is attractive for the dual-mode resonator. Interestingly, C not only affects the dual-resonant frequencies f_o and f_e, but also relates to the tuning range of f_o. Equation (2) points out that if C_o has a fixed range, C will influence f_o and its tuning range. Here, presuming $C_o \in (C_{o1}, C_{o2})$. In order to simplify the analysis process, two extreme derivations about C are shown as follows.

Case 1: If C tends to the positive infinity ($+\infty$), Equation (2) can be rewritten as

$$\lim_{C \to +\infty} f_o = 0. \quad (3)$$

It is assumed that the maximum and minimum of f_o are f_{o1} and f_{o2} for C_{o1} and C_{o2}, respectively, where $f_{o1} > f_{o2}$. Equation (3) always has two meanings: 1) f_o will reduce to zero, 2) $f_{o1} - f_{o2}$ will become narrow and gradually closes to zero along with the growth of C.

Case 2: If C approaches to zero, Equation (2) is expressed as

$$f_o = \frac{Y_1 Y_2 - Y_1^2 \tan^2(2L\beta_o)}{4\pi C_o (Y_1 + Y_2)\tan(2L\beta_o)}. \tag{4}$$

The tuning range of f_o is from f_{o3} to f_{o4} at C_{o1} and C_{o2}, respectively, where $f_{o3} > f_{o4}$. Inspection of Equation (4), it implies that f_o is larger than that in Equation (3), and the frequency difference $f_{o3} - f_{o4}$ is $\gg 0$.

To sum up, as $C_o \in (C_{o1}, C_{o2})$, it can deduce

$$f_{o3} - f_{o4} > f_{o1} - f_{o2}. \tag{5}$$

In spite that C is extremely supposed for simplicity in analysis, Equations (3) - (5) are valid for general C and give a useful conclusion: if the interval of variable C_o is defined, the tuning range of f_o reduces as C enlarges. Also, the decreasing of f_o is accompanied by the growth of C, and the same conclusion for f_e and C can be obtained from Equation (1). However, C has little effect on the tuning range of f_e, since the frequency difference of f_e is almost unchanged.

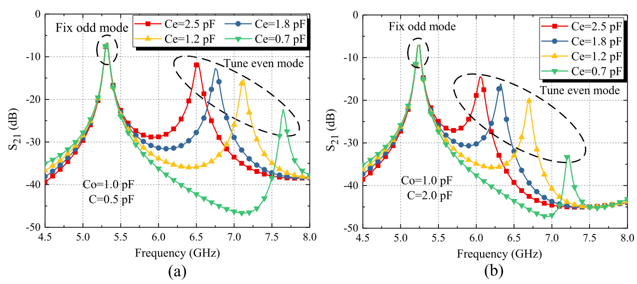

FIGURE 3. Fix C_o and tune C_e at (a) c = 0.5 pF and (b) c = 2.0 pF.

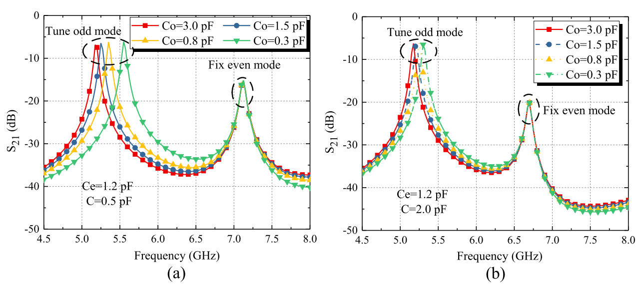

FIGURE 4. Fix C_e and tune C_o at (a) c = 0.5 pF and (b) c = 2.0 pF.

To verify deductions above, a series of simulations are performed. Figs. 3 and 4 show the simulated results of Fig. 2(a) for the tunable f_e and f_o, respectively, when $W_1 = 0.6$ mm, $W_2 = 1.2$ mm, $S = 0.2$ mm, and $L = 4.0$ mm. As can be observed, f_o and f_e can be individually tuned by corresponding variable capacitor and have no effect on each other. The

TABLE 1. Comparison in range for different C, C_e and C_o.

f (GHz) / C (pF)	C_e (pF)	C_o (pF)	Range (GHz)	
	0.7 — 2.5	0.3 — 3.0	f_e	f_o
0.5	7.65 — 6.5	5.55 — 5.17	1.15	0.38
2.0	7.2 — 6.05	5.3 — 5.17	1.15	0.13

performance comparisons for various values C, C_o and C_e are summarized in Table 1. These results manifest that C is a key parameter to determine f_e and f_o. Moreover, a small C or the wide C_o and C_e can expand the tuning ranges of the dual-resonant frequencies. Hence, loading proper C at the two ends of the loop is a feasible solution to reduce the circuit sizes and extend the tuning ranges. More importantly, it should adopt high-precision capacitor C as much as possible to make sure all of C in resonator are same for validation of the odd- and even-mode analysis method.

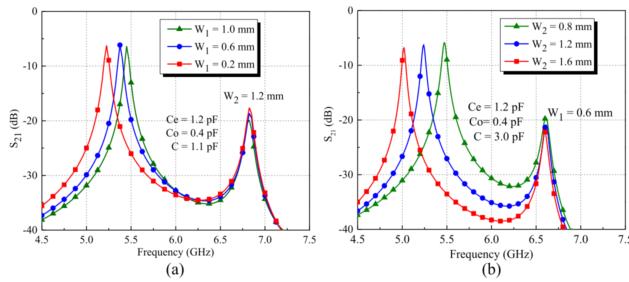

FIGURE 5. f_o varies and f_e is unchanged. (a) Fix W_2 and tune W_1 at $C =$ 1.1 pF. (b) Fix W_1 and tune W_2 at $C = 3.0$ pF.

Besides, the structure of the SI dual-mode resonator with $Y_1 \neq Y_2$ has two advantages. One advantage is that the SI resonator introduces a method of changing the frequency spacing $f_e - f_o$. Fig. 5 denotes the relationship between different W_1, W_2, f_o and f_e. The $f_e - f_o$ increases with the decreasing of the width ratio W_1/W_2, which is convenient to manage $f_e - f_o$. The other advantage is that the variation of W_1 or W_2 can only tune f_o and is incapable of adjusting f_e, thus adding a way to freely change f_o. As shown in Fig. 5(a), f_o is tuned by W_1 while f_e is unaltered. The same conclusion can be drawn from Fig. 5(b).

C. DESIGN OF THE INDEPENDENT TUNABLE DUAL-BAND BPF

Instead of employing the one-pole square open-loop SI dual-mode resonator with the low band-to-band isolation and spurious suppression, a three-pole elliptic-function filter [12] is applied to design the dual-band BPF. As can be seen in Fig. 6(a), the dual-band BPF is composed of five identical square open-loop SI resonators, but only the central one has an independent dual-mode operation, whereas other resonators provide either odd mode or even mode to restrain harmonic-mixing products. The main operating principle of the dual-band BPF is that the central resonator combined with

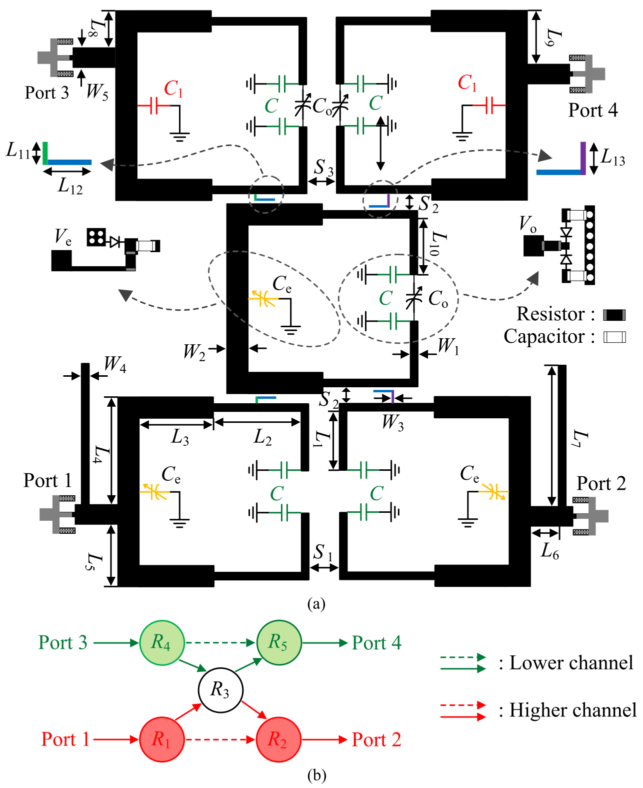

FIGURE 6. (a) The layout and (b) coupling theory of the concurrent dual-band BPF.

two upper resonators is implemented to generate f_o and limit f_e by a special capacitor C_1, and the central one combined with two lower resonators is used to produce f_e and hold back f_o through the corresponding quarter-wave lines L_7. Fig. 6(b) interprets the detailed coupling theory of the dual-band BPF. Specifically, the port 1 (port 3) and port 2 (port 4) are utilized to extract the f_e (f_o) as the higher (lower) frequency channel.

The center frequency of the higher (lower) channel is 7.8 GHz (5.2 GHz) with a bandwidth 300 MHz (200 MHz), and the initial values of the used capacitors are $C = 1.8$ pF and $C_o = C_e = 0.23$ pF. To determine the physical dimensions of the dual-band BPF on the Rogers 4350B substrate with a ε_r of 3.66 and a thickness of 0.508 mm, the design procedures are summarized as follows.

1) Generate 3-order coupling matrixes and external quality factors of the dual-band BPF by filter synthesis as

$$\left[M^L\right] = \begin{bmatrix} M_{44} & M_{43} & M_{45} \\ M_{34} & M_{33} & M_{35} \\ M_{54} & M_{53} & M_{55} \end{bmatrix} = \begin{bmatrix} 0.122 & 0.712 & 0.600 \\ 0.712 & -0.634 & 0.712 \\ 0.600 & 0.712 & 0.122 \end{bmatrix}, \tag{6}$$

$$\left[M^H\right] = \begin{bmatrix} M_{11} & M_{13} & M_{12} \\ M_{31} & M_{33} & M_{32} \\ M_{21} & M_{23} & M_{22} \end{bmatrix} = \begin{bmatrix} 0.084 & 0.989 & 0.337 \\ 0.989 & -0.327 & 0.989 \\ 0.337 & 0.989 & 0.084 \end{bmatrix}, \tag{7}$$

$$Q_e^L = 29 \quad Q_e^H = 22.19, \tag{8}$$

where M_{ij} stands for the coupling coefficient between the resonator R_i and R_j ($i, j = 1, 2, 3, 4, 5$), Q_e is the external quality factor, and the mark L and H represent the lower and higher frequency channel, respectively.

2) Calculate L roughly based on $f = (f_e + f_o)/2$, and then compute Y_1 (W_1) and Y_2 (W_2) according to (1) - (2).

3) Use (6) - (8) and carry out co-simulation to acquire the L_5, L_8, L_9, S_1, S_2 and S_3 in the ADS based on equation [11]

$$M_{i,j} = \pm\frac{1}{2}\left(\frac{f_{0i}}{f_{0j}} + \frac{f_{0j}}{f_{0i}}\right)\sqrt{\left(\frac{f_{pi}^2 - f_{pj}^2}{f_{pi}^2 + f_{pj}^2}\right) - \left(\frac{f_{0i}^2 - f_{0j}^2}{f_{0i}^2 + f_{0j}^2}\right)}$$
$$Q_E = \omega\tau/4, \tag{9}$$

where f_{0i} and f_{0j} ($i, j = 1, 2, 3, 4, 5$) mean the self-resonant frequency of each resonator, respectively; f_{pi} and f_{pj} represent the split resonant frequencies when two resonators couple to each other; ω is the resonant angular frequency and τ is the group delay of the input or output.

4) Take a trade-off between L and C so as to achieve a wide tuning range as discussed in the Section B.

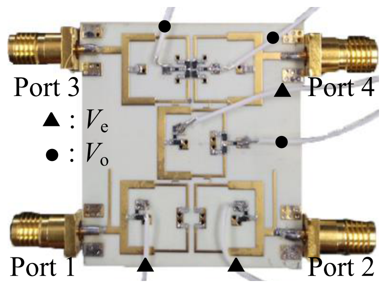

Unit: mm

L_1	L_2	L_3	L_4	L_5	L_6
3.3	4.7	4.0	6.82	3.0	1.4
L_7	L_8	L_9	L_{10}	L_{11}	L_{12}
8.5	2.0	3.0	3.1	0.4	1.0
L_{13}	W_1	W_2	W_3	W_4	W_5
0.8	0.4	1.2	0.12	0.4	1.08
S_1	S_2	S_3	C = 1.8 pF		
0.82	0.55	0.7	C_1 = 3.0 pF		

FIGURE 7. The fabricated concurrent dual-band BPF with its physical dimensions.

The fabricated dual-band BPF and its physical sizes are shown in Fig. 7. Varactor diodes SMV2201-040LF (0.23-2.1 pF) are used for the variable capacitors and the Agilent network analyzer N5230C is used for measurement. Fig. 8 (Fig. 9) shows the simulated and measured S_{43} (S_{21}) for the lower (higher) frequency channel, which is individually managed by the tuning voltage V_o (V_e). The undesired channel could be attenuated by 20 dB in the operating channel. In addition, the attenuation will be larger if the band-to-band isolation from port 1 (port 2) to port 4 (port 3) is considered, as illustrated in Fig. 10. The measured band-to-band isolation is > 26 dB for the low frequency channel and > 40 dB for the higher frequency channel, respectively. From these results, it would be beneficial to prevent each oscillation frequency from coupling to the other transistor and diminish harmonic-mixing products, thus resulting in a pure spectrum output for the concurrent dual-band VCO. Slight discrepancies between the simulated and measured results are mainly attributed to

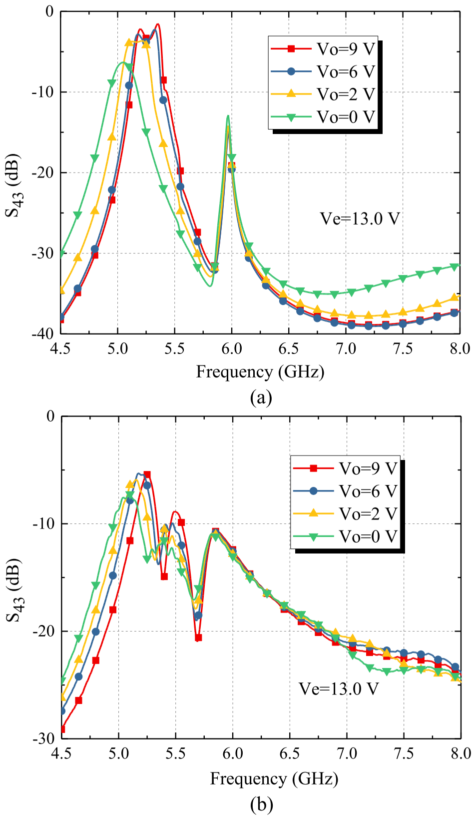

FIGURE 8. (a) Simulated and (b) measured results of the lower frequency channel.

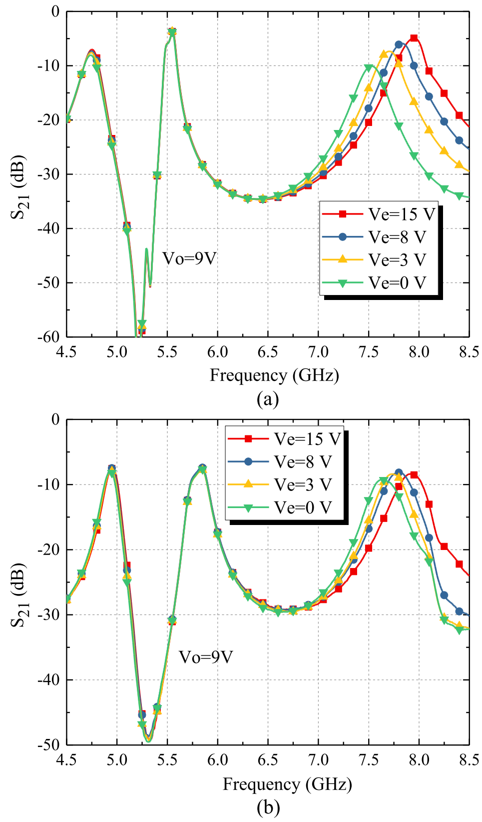

FIGURE 9. (a) Simulated and (b) measured results of the higher frequency channel.

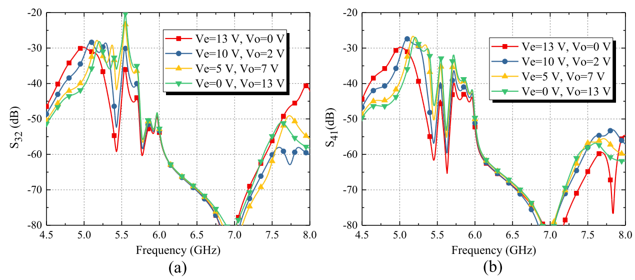

FIGURE 10. Measured results of the (a) S_{32} and (b) S_{41}.

parasitic capacitance effects from the weld of C_o and the approximate SPICE model of the used varactor diodes.

III. CONCURRENT DUAL-BAND VCO FABRICATION AND MEASURMENT

To extend the independently controllable dual-band BPF to a concurrent dual-band VCO, two parallel-feedback structures are chosen to design separate oscillation systems with two different output ports. The fabricated concurrent dual-band VCO is shown in Fig. 11 with a physical size of 5.3 × 3.7 mm^2. It contains a dual-band BPF, two transistors and the input and output matching circuits. The matching circuits make the transistor supply a suitable gain and a loop phase to meet the demands of the parallel-feedback oscillation criteria (total loop gain $G > 1$ and total phase shift of the oscillator loop $\theta = 360^o$). Two transistors BFU730 are selected as the amplifiers to provide gains in the loops. The total dc power consumption of a transistor biased at a collector-emitter voltage 2.1 V with a collector current of 9.7 mA is 20.37 mW.

Figs. 12 and 13 show the measured oscillation frequencies, phase noises, and output powers of the concurrent dual-band VCO versus the tuning voltages. When V_o varies from 0 to 12 V, as seen from Fig. 12(a), the lower oscillation frequency increases from 5.114 to 5.28 GHz with a tuning range of 166 MHz. The output power alters from 5.2 to 8.9 dBm with a 3.7 dB variation over the tuning frequency range. In addition, the phase noise deteriorates from −130.6 to −114.8 dBc/Hz at 1-MHz offset frequency and −103.9 to −92.4 dBc/Hz at 100-KHz offset frequency, respectively. Similarly, as shown in Fig. 12(b), the higher oscillation frequency ranges from 7.61 to 7.97 GHz (tuning range 360 MHz) with the tuning voltage V_e between 0 and 13 V. The output power increases from −3.98 to 4.56 dBm with a 8.54 dB difference during the whole tuning range. Furthermore, when V_e exceeds 13 V, the tuning frequency changes a little. The phase noises at 1-MHz and 100-KHz offset varie from −126.3 to −121.4 dBc/Hz and −98.6 to −93.6 dBc/Hz, respectively.

In order to intuitively display two oscillation frequencies on the Agilent spectrum analyzer N9030A, two input ports of the T-type connector are adopted to connect the outputs of the

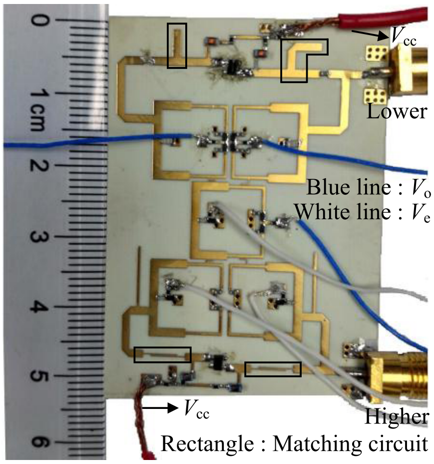

FIGURE 11. Photograph of the proposed concurrent dual-band VCO.

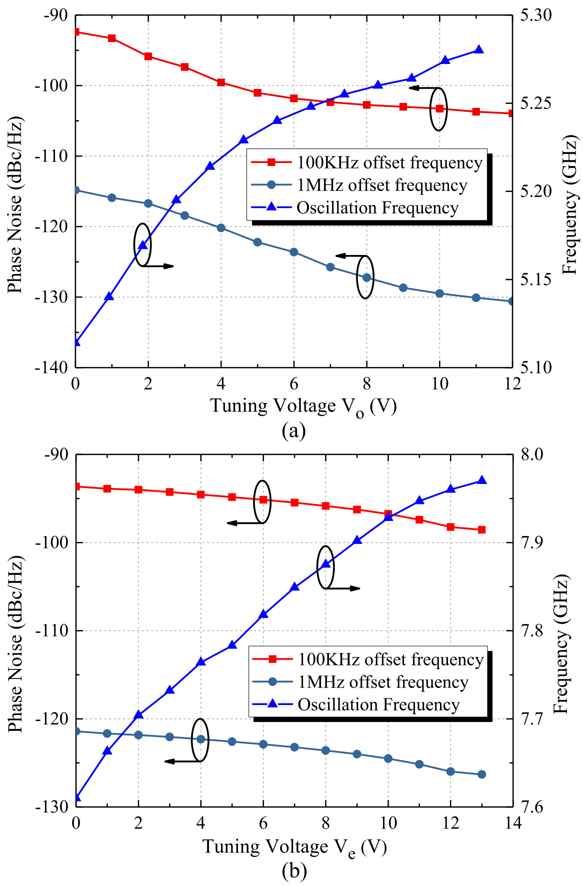

FIGURE 12. Measured results of phase noises and oscillation frequencies (a) for the lower oscillation frequency and (b) for the higher oscillation frequency.

fabricated dual-band VCO, and the output of the connector is linked with the N9030A. In the case of tuning voltage $V_o = 0$ V and $V_e = 13$ V, the measured dual-band spectrum output has been shown in Fig. 14, where the two oscillation frequencies are 5.114 (f_1) and 7.97 (f_2) GHz with the output powers of 5.2 and 3.02 dBm, respectively. Since a good band-

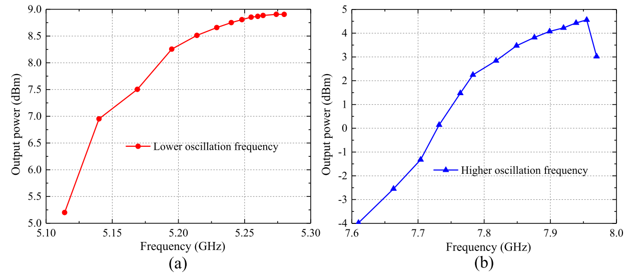

FIGURE 13. Output powers of the concurrent dual-band VCO. (a) Lower oscillation frequency. (b) Higher oscillation frequency.

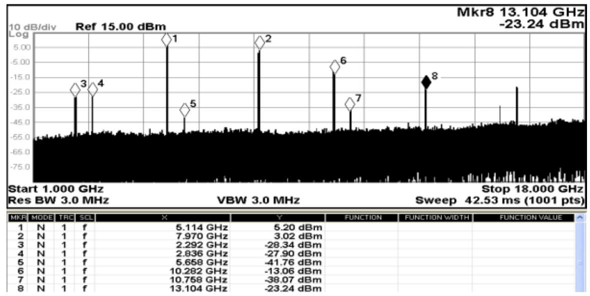

FIGURE 14. Measured output spectrum of the f_1 and f_2.

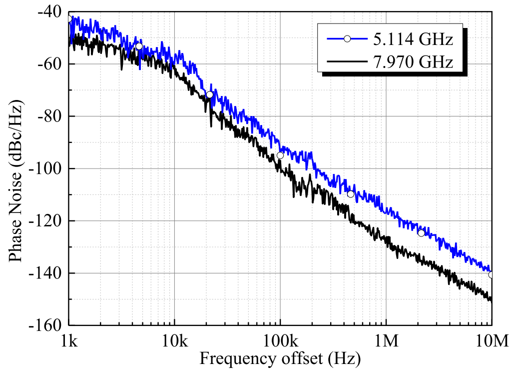

FIGURE 15. Measured phase noises of the f_1 and f_2.

to-band isolation between the lower and higher frequency channel, the suppression of main harmonic-mixing signal happening at 5.658 GHz ($2f_2 - 2f_1$) is < -41.76 dBm, which denotes the harmonic characteristics of dual-band VCO are $>$ 46.96 (5.2 + 41.76) dBc for the around-carrier frequencies. Besides, other harmonic-mixing products, such as 2.836 GHz ($f_2 - f_1$), 2.292 GHz ($2f_1 - f_2$), 10.282 GHz ($2f_1$), 10.758 GHz ($2f_2 - f_1$) and 13.104 GHz ($f_1 + f_2$), are neglected because of small magnitudes or far distances compared with the f_1 and f_2. Finally, the measured phase noises of f_1 and f_2 are displayed in Fig. 15.

To make a fair comparison for the various oscillators and VCOs, the figure-of-merit (FOM) can be calculated as [6]

$$\text{FOM} = L(\Delta f) - 20\log_{10}\left(\frac{f_0}{\Delta f}\right) + 10\log_{10}\left(\frac{P_{DC}}{1mW}\right), \quad (10)$$

where $L(\Delta f)$ is the phase noise at the offset frequency Δf, f_0 is the oscillation frequency, and P_{DC} is the dc power

TABLE 2. Comparison in performances for the proposed dual-band VCO and other reported ones.

Ref	Frequency (GHz)	Concurrence	P_{out} (dBm)	Tuning range (%)	Phase noise (dBc/Hz)	FOM (dBc/Hz)	IM Suppression (dBc)	I	Size (mm^2)
[13]	8.0	N	10.0	N	-150.0@1MHz	-205.0	N	N	$2.88\lambda_g \times 2.15\lambda_g$ (f = 8.0 GHz)
[14]	9.1	N	9.7	N	-138.0@1MHz	-205.13	N	N	$1.83\lambda_g \times 1.14\lambda_g$ (f = 9.1 GHz)
[15]	2.46	N	3.38	0.8	-147.92@1MHz	-203.18	N	N	$0.74\lambda_g \times 0.4\lambda_g$ (f = 2.46 GHz)
[4]	8.29	Y	-20.34	N	-107.0@100KHz	-192.37	<-30/-15 @ $3f_1 - f_2$	N	N
	15.00		-8.23		-103.0@100KHz	-193.52			
[5]	3.36	Y	-9.99	N	-120.83@9.8MHz	N	<-2.68 @ $f_2 - f_1$	N	N
	5.24		-15.8		-93.80@100KHz				
[6]	1.85	Y	5.37	N	-120.84@1MHz	-172.57	<-50 @ $2f_1 - 2f_2$	N	$0.75\lambda_g \times 0.67\lambda_g$ (f = 1.85 GHz)
	2.66		6.80		-121.70@1MHz	-177.23			
[7]	4.18	Y	-0.87	N	-112.30@100KHz	-188.7	<-35 @ $2f_1 - f_2$ / $2f_2 - f_1$ <-24 @ $f_1 + f_2$ / $f_1 - f_2$	N	$1.56\lambda_g \times 1.23\lambda_g$ (f = 4.18 GHz)
	5.49		5.38		-110.30@100KHz	-189.1			
[8]	2.64	Y	-4.34	8.75	-127.1@1MHz	-190.4	N	N	N
	6.85		-6.02	10.01	-123.4@1MHz	-194.7			
This work	**5.28**	**Y**	**8.9**	**3.19**	**-130.6@1MHz**	**191.96**	**<-46.96 @ $2f_2 - 2f_1$**	**Y**	**$1.53\lambda_g \times 1.09\lambda_g$ (f = 5.28 GHz)**
	7.97		**3.02**	**4.62**	**-126.31@1MHz**	**-191.23**			

I = independently tunable two oscillation frequencies, Y / N = Yes / No, λ_g = guide wavelength.

consumption (mW). For the lower oscillation frequency, the FOM varies from −173.48 to −185.26 and −175.89 to −191.96 dBc/Hz for 100-KHz and 1-MHz offset, respectively. For the higher oscillation frequency, the FOM adjusts from −178.14 to −183.54 and −185.94 to −191.23 dBc/Hz for 100- KHz and 1-MHz offset, respectively. The best FOM of the dual-band VCO is −191.96 dBc/Hz with a phase noise −130.6 dBc/Hz at 1-MHz offset frequency for 5.28 GHz. Performance comparisons of the proposed dual-band VCO with other reported ones are summarized in Table 2. From Table 2, it is clear that a concurrent VCO with independent dual-band operation has been performed in this paper.

IV. CONCLUSION

This paper develops a concurrent dual-band VCO with flexible tunable characteristic based on the filtering square open-loop dual-band BPF. The principal technique is that two types of varactor diodes can individually control the odd-even resonant frequencies of the dual-band BPF, which is applied for realizing the independent tuning of the two oscillation frequencies. Also, the sufficient band-to-band isolation and good spurious suppression are necessarily required in the design of concurrent dual-band VCO. Moreover, the derived expressions contribute to the performance optimization in terms of size miniaturization and tuning range expansion. Therefore, the novel concurrent dual-band VCO is expected to be widely utilized in the modern multi-band wireless communication systems.

REFERENCES

[1] Z.-Z. Chen and T.-C. Lee, "The study of a dual-mode ring oscillator," *IEEE Trans. Circuits Syst. II, Exp. Briefs.*, vol. 58, no. 4, pp. 210–214, Apr. 2011.

[2] M. M. Bajestan, V. D. Rezaei, and K. Entesari, "A low phase-noise wide tuning-range quadrature oscillator using a transformer-based dual-resonance ring," *IEEE Trans. Microw. Theory Techn.*, vol. 63, no. 4, pp. 1142–1153, Apr. 2015.

[3] S. Jain, S. L. Jang, and N. T. Tchamov, "Oscillation mode swapping dual-band VCO," *IEEE Microw. Wireless Compon. Lett.*, vol. 26, no. 3, pp. 210–212, Mar. 2016.

[4] Y. Liu, X.-H. Tang, T. Wu, L. Wang, and F. Xiao, "A SIW-based concurrent dual-band oscillator," in *Proc. IEEE Int. Conf. Microw. Millim. Wave Technol.*, May 2012, pp. 1–4.

[5] B. Iyer, A. Kumar, and N. P. Pathak, "3.36-/15.24-GHz concurrent dual-band oscillator for WiMAX/WLAN applications," in *Proc. IEEE MTT-S Microw. RF Conf.*, Dec. 2013, pp. 1–4.

[6] B. Li, Y. Liu, C. Yu, and Y. Wu, "A novel concurrent dual-band oscillator based on a single ring resonator," *IEEE Microw. Wireless Compon. Lett.*, vol. 26, no. 8, pp. 607–609, Aug. 2016.

[7] Z. Yang, J. Dong, B. Luo, T. Yang, and Y. Liu, "Low phase noise concurrent dual-band oscillator using compact diplexer," *IEEE Microw. Wireless Compon. Lett.*, vol. 25, no. 10, pp. 672–674, Oct. 2015.

[8] S. Jain, S. L. Jang, and N. T. Tchamov, "Tuned LC-resonator dual-band VCO," *IEEE Microw. Wireless Compon. Lett.*, vol. 26, no. 3, pp. 204–206, Mar. 2016.

[9] A. Li and H. C. Luong, "A reconfigurable 4.7–6.6 GHz and 8.5–10.7 GHz concurrent and dual-band oscillator in 65 nm CMOS," in *Proc. IEEE Radio Freq. Integr. Circuits Symp.*, Jun. 2012, pp. 523–526.

[10] B. Q. Li, Y. A. Liu, C. P. Yu, and Y. L. Wu, "Independent control function for concurrent dual-band VCO," *IEEE Microw. Wireless Compon. Lett.*, to be published, doi: 10.1109/LMWCL.2018.2803109.

[11] X. Huang, L. Zhu, Q. Feng, Q. Xiang, and D. Jia, "Tunable bandpass filter with independently controllable dual passbands," *IEEE Trans. Microw. Theory Techn.*, vol. 61, no. 9, pp. 3200–3208, Sep. 2013.

[12] J.-S. Hong and M. J. Lancaster, *Microstrip Filters for RF/Microwave Applications*. New York, NY, USA: Wiley, 2001, pp. 331–339.

[13] J. Choi and A. Mortazawi, "A new *X*-band low phase-noise multiple-device oscillator based on the extended-resonance technique," *IEEE Trans. Microw. Theory Techn.*, vol. 55, no. 8, pp. 1642–1648, Aug. 2007.

[14] M. Nick and A. Mortazawi, "Low phase-noise planar oscillators based on low-noise active resonators," *IEEE Trans. Microw. Theory Techn.*, vol. 58, no. 5, pp. 1133–1139, May 2010.

[15] C.-H. Tseng and T.-S. Huang, "Microwave voltage-controlled oscillator with harmonic-suppressed stepped-impedance-resonator filter," *IEEE Trans. Circuits Syst. II, Exp. Briefs.*, vol. 64, no. 5, pp. 520–524, May 2017.

BOQIONG LI received the B.S. and M.S. degrees in communication engineering from Lanzhou University, Lanzhou, China, in 2011 and 2014, respectively. He is currently pursuing the Ph.D. degree in electrical engineering from the Beijing University of Posts and Telecommunications, Beijing, China.

His current research interests include microwave components and wireless systems design.

YONGLE WU (M'12–SM'15) received the B.Eng. degree in communication engineering and the Ph.D. degree in electronic engineering from the Beijing University of Posts and Telecommunications (BUPT), Beijing, China, in 2006 and 2011, respectively.

In 2010, he was a Research Assistant with the City University of Hong Kong, Kowloon, Hong Kong. In 2011, he joined BUPT, where he is currently a Full Professor with the School of Electronic Engineering. His research interests include microwave components and wireless systems design.

CUIPING YU received the B.S. degree in communication engineering from Jilin University, Jilin, China, in 2004, and the Ph.D. degree in electronic engineering from the Beijing University of Posts and Telecommunications (BUPT), Beijing, China, in 2010.

Since 2013, she has been an Associate Professor with the School of Electronic Engineering, BUPT. Her research interests include nonlinear modeling and linearization of transmitters/power amplifiers, high efficiency power amplifiers design, and multi-band components design.

YUANAN LIU received the B.S., M.S., and Ph.D. degrees in electrical engineering from the University of Electronic Science and Technology of China, Chengdu, China, in 1984, 1989, and 1992, respectively.

In 1984, he joined the 26th Institute of Electronic Ministry of China to develop the inertia navigating system. In 1992, he began his first post-doctoral position at the EMC Lab, Beijing University of Posts and Telecommunications (BUPT), Beijing, China. In 1995, he started his second post-doctoral position at the Broadband Mobile Laboratory, Department of System and Computer Engineering, Carleton University, Ottawa, ON, Canada. Since 1997, he has been a Professor with the Wireless Communication Center, College of Telecommunication Engineering, BUPT, where he is involved in the development of next-generation cellular system, wireless LAN, Bluetooth application for data transmission, EMC design strategies for high speed digital system, and EMI and EMS measuring sites with low cost and high performance.